

isotope effect that has any quantitative meaning within the context of simple BCS superconductivity.

We have argued that our observed reduced total isotope coefficient is the result of a large Coulomb repulsion resulting in a large value of  $\mu^*$ . Certainly, many other causes for a reduced total isotope effect can occur—for example, anharmonic lattice vibration could affect the mass dependence of  $\langle\omega\rangle$ , or complex dimensional effects on the Fermi surface could affect  $f(\lambda, \mu^*)$ . The model of An and Pickett<sup>6</sup>, for example, might lead to a reduced total isotope effect if the two-dimensional nature of the hole band is found to have an effect on  $\lambda$  or  $\mu^*$ . This difference between the measured total isotope effect and 1/2 may appear insignificant, but the cause of this discrepancy may be in some way related to the high  $T_c$  observed in this material. Although it is possible to calculate  $T_c$  for MgB<sub>2</sub> based on reasonable choices of parameters using the McMillan equation, correctly modelling  $\alpha_t$  (and  $\alpha_{Mg}$  and  $\alpha_B$ ) may place constraints on these calculations that will provide important insight into how such a high  $T_c$  is achieved in this simple *sp* metal.

*Note added in proof:* The reduced isotope effect in MgB<sub>2</sub> has recently been explained<sup>22</sup> as being due to the large anharmonicity of the E<sub>2g</sub> mode. If correct, this would reduce the value of  $\lambda$  and  $\mu^*$  required to account for the high  $T_c$  of the material. □

Received 8 March; accepted 25 April 2000.

- Nagamatsu, J., Nakagawa, N., Muranaka, T., Zenitani, Y. & Akimitsu, J. Superconductivity at 39 K in magnesium diboride. *Nature* **410**, 63–64 (2001).
- Bud'ko, S. L. *et al.* Boron isotope effect in superconducting MgB<sub>2</sub>. *Phys. Rev. Lett.* **86**, 1877–1880 (2001).
- Cooper, A. S., Corenzwit, E., Longinotti, L. D., Matthias, B. T. & Zachariasen, W. H. Superconductivity: the transition temperature peak below four electrons per atom. *Proc. Natl Acad. Sci. USA* **67**, 313–319 (1970).
- Leyarovska, L. & Leyarovski, E. A search for superconductivity below 1K in transition metal borides. *J. Less Common Met.* **67**, 249–255 (1979).
- Kortus, J., Mazin, I. I., Belashchenko, K. D., Antropov, V. P. & Boyer, L. L. Superconductivity of metallic boron in MgB<sub>2</sub>. Preprint cond-mat/0101446 at (<http://xxx.lanl.gov>) (2001).
- An, J. M. & Pickett, W. E. Superconductivity of MgB<sub>2</sub> from hole-doped covalent bonds. Preprint cond-mat/0102391 at (<http://xxx.lanl.gov>) (2001).
- Kostic, P. *et al.* Paramagnetic Meissner effect in Nb. *Phys. Rev. B* **53**, 791–801 (1996).
- Lawrie, D. D. & Franck, J. P. Boron isotope effect in Ni and Pd based borocarbide superconductors. *Physica C* **245**, 159–163 (1995).
- Cheon, K. O., Fisher, I. R. & Canfield, P. C. Boron isotope effect in single-crystal YNi<sub>2</sub>B<sub>2</sub>C and LuNi<sub>2</sub>B<sub>2</sub>C superconductors. *Physica C* **312**, 35–39 (1999).
- Allen, P. B. & Dynes, R. C. Transition temperature of strong-coupled superconductors reanalyzed. *Phys. Rev. B* **12**, 905–922 (1975).
- McMillan, W. L. Transition temperature of strong-coupled superconductors. *Phys. Rev.* **167**, 331–344 (1968).
- Garland, J. W. Jr. Isotope effect in superconductivity. *Phys. Rev. Lett.* **11**, 114–119 (1963).
- Carbotte, J. P. Properties of boson-exchange superconductors. *Rev. Mod. Phys.* **62**, 1027–1157 (1990).
- Osborn, R., Goremychkin, E. A., Kolesnikov, A. I. & Hinks, D. G. Phonon density-of-states in MgB<sub>2</sub>. *Phys. Rev. Lett.* (in the press); also as preprint cond-mat/0103064 at (<http://xxx.lanl.gov>) (2001).
- Kremer, R. K., Gibson, B. J. & Ahn, K. Heat capacity of MgB<sub>2</sub>: Evidence for moderately strong coupling behavior. Preprint cond-mat/0102432 at (<http://xxx.lanl.gov>) (2001).
- Kotegawa, H., Ishida, K., Kitaoka, Y., Muranaka, T. & Akimitsu, J. Evidence for strong-coupling s-wave superconductivity in MgB<sub>2</sub>: <sup>11</sup>B NMR study. Preprint cond-mat/0102334 at (<http://xxx.lanl.gov>) (2001).
- Rubio-Bollinger, G., Suederow, H. & Vieira, S. Tunneling spectroscopy in small grains of superconducting MgB<sub>2</sub>. Preprint cond-mat/0102242 at (<http://xxx.lanl.gov>) (2001).
- Karapetrov, G., Iavarone, M., Kwok, W. K., Crabtree, G. W. & Hinks, D. G. Scanning tunneling spectroscopy in MgB<sub>2</sub>. *Phys. Rev. Lett.* (in the press); also as preprint cond-mat/0102312 at (<http://xxx.lanl.gov>) (2001).
- Schmidt, H., Zasadzinski, J. F., Gray, K. E. & Hinks, D. G. Energy gap from tunneling and metallic Shubnikov contacts into MgB<sub>2</sub>: evidence for a weakened surface layer. *Phys. Rev. B* (in the press); also as preprint cond-mat/0102389 at (<http://xxx.lanl.gov>) (2001).
- Sharoni, A., Felner, I. & Millo, O. Tunneling spectroscopy and magnetization measurements of the superconductor properties of MgB<sub>2</sub>. *Phys. Rev. B* (in the press); also as preprint cond-mat/0102325 at (<http://xxx.lanl.gov>) (2001).
- Kong, Y., Dolgov, O. V., Jepsen, O. & Anderson, O. K. Electron-phonon interaction in the normal and superconducting states of MgB<sub>2</sub>. *Phys. Rev. B* (in the press); also as preprint cond-mat/0102499 at (<http://xxx.lanl.gov>) (2001).
- Yildirim, T. *et al.* Giant anharmonicity and non-linear electron-phonon coupling in Mg B<sub>2</sub>: combined first principles calculations and neutron scattering study. Preprint cond-mat/0103469 at (<http://xxx.lanl.gov>) (2001).

#### Acknowledgements

This work was supported by the US Department of Energy, Office of Science.

Correspondence and requests for materials should be addressed to D.G.H. (e-mail: hinks@anl.gov).

## Constraints on hydrothermal processes and water exchange in Lake Vostok from helium isotopes

Philippe Jean-Baptiste\*, Jean-Robert Petit†, Vladimir Ya. Lipenkov‡, Dominique Raynaud† & Nartsiss I. Barkov‡

\* Laboratoire des Sciences du Climat et de l'Environnement, CEA/CNRS, Centre d'études de Saclay, 91191 Gif sur Yvette, France

† Laboratoire de Glaciologie et de Géophysique de l'Environnement, CNRS, Grenoble, 38402 Saint Martin d'Hères, France

‡ Arctic and Antarctic Research Institute, Beringa Street 38, 199397 St Petersburg, Russia

Lake Vostok, the largest subglacial lake in Antarctica, is covered by the East Antarctic ice sheet, which varies in thickness between 3,750 and 4,100 m (ref. 1). At a depth of 3,539 m in the drill hole at Vostok station, sharp changes in stable isotopes and the gas content of the ice delineate the boundary between glacier ice and ice accreted through re-freezing of lake water<sup>2</sup>. Unlike most gases, helium can be incorporated into the crystal structure of ice during freezing<sup>3</sup>, making helium isotopes in the accreted ice a valuable source of information on lake environment. Here we present helium isotope measurements from the deep section of the Vostok ice core that encompasses the boundary between the glacier ice and accreted ice, showing that the accreted ice is enriched by a helium source with a radiogenic isotope signature typical of an old continental province. This result rules out any significant hydrothermal energy input into the lake from high-enthalpy mantle processes, which would be expected to produce a much higher <sup>3</sup>He/<sup>4</sup>He ratio. Based on the average helium flux for continental areas, the helium budget of the lake leads to a renewal time of the lake of the order of 5,000 years.

In the upper part of the Antarctic ice sheet, helium is of atmospheric origin<sup>4</sup>. Previous measurements obtained between 1989 and 1992 at various depths—from 116 to 2,501 m (Table 1)—in the Vostok ice core indicate a nearly constant helium concentration: [He] = 12.1 ± 1.3 nmol kg<sup>-1</sup>, with an isotopic ratio  $R = (0.97 \pm 0.03)R_a$ , where  $R = {}^3\text{He}/{}^4\text{He}$  and  $R_a$  is the atmospheric ratio ( $1.38 \times 10^{-6}$ ). The measured concentration represents only a fraction of the helium initially present in the air bubbles at the pores' close-off (21.4–22.3 nmol kg<sup>-1</sup> at Vostok<sup>4</sup>) owing to the upward diffusion of helium to the atmosphere as the air bubbles are increasingly compressed<sup>5</sup>. In deeper layers, the helium isotope distribution may be influenced by the radiogenic signature from the bedrock<sup>6</sup>. In Lake Vostok, dissolved helium may therefore have three main possible origins: (1) atmospheric helium, with an isotope ratio close to  $R_a$ , trapped in glacier ice and released into the lake water as the basal layers are melted; (2) radiogenic crustal helium produced by the decay of U and Th in the bedrock and bottom sediments, characterized by  $R < 0.05R_a$  (refs 7,8); and (3) mantle helium with  $R > 8R_a$  (refs 8–10). (We note that, because of the large ice–gas age difference at pore close-off in central Antarctica, of the order of 1,000 years or greater, there should be no imprint of any tritiogenic <sup>3</sup>He produced by the decay of natural tritium.)

We analysed 14 new samples from the Vostok ice core from a depth range of 3,530–3608 m (Table 1), which encompasses the transition between glacier ice and the refrozen lake water at 3,539 m depth. The main feature of the helium isotope distribution with depth (Fig. 1) is the pronounced difference in both the helium concentration and isotope ratio between glacier ice and the refrozen lake water. For depths between 3,530 and 3,535 m, the mean helium concentration, [He] = 10.0 ± 1.3 nmol kg<sup>-1</sup>, is similar to

that measured in the upper layers of the Vostok ice core, with  $R = (1.03 \pm 0.08)R_a$ , close to the atmospheric value. Below 3,539 m depth, the helium content of the samples is enriched by a factor of 3 with respect to glacier ice ( $[He] = 33.9 \pm 2.6 \text{ nmol kg}^{-1}$ ) and exhibits a clear radiogenic signature,  $R = (0.25 \pm 0.04)R_a$ , typical of old stable continental provinces.

Lake Vostok's ice ceiling is tilted, with an ice thickness of 4,300 m in the north and 3,750 m in the south. This north–south gradient of the pressure-dependent melting point favours glacier ice melting in the north and lake water refreezing in the south<sup>11,12</sup>, where the Vostok station is located. Radar studies also suggest basal melting on the western margin upstream from Vostok<sup>11</sup>; however, the numerous solid inclusions observed in the upper part of the lake ice in the Vostok core indicate that freezing may indeed occur as soon as glacial ice loses contact with bedrock<sup>2</sup>. Water influx also occurs as a result of ice melting off the base of the glacier over the lake catchment in response to geothermal flux and shear-strain heating.

The long-term mass balance between the input of melt water and the accreted ice export allows us to determine the helium isotope budget of the lake. Per unit of time, the amount of helium released to the lake by the melted glacier ice (with a helium concentration  $C_{He1}^{in}$ ) and basal water runoff (with a helium concentration  $C_{He2}^{in}$ ), together with the amount of crustal helium injected into the lake from the bedrock ( $Q_{He}$ ), must be balanced by the amount of helium that leaves the lake by direct diffusion through the glacier ice/lake ice interface ( $Q_{He}^{dif}$ ), together with the exported lake ice of helium concentration  $C_{He}^{out}$ . This leads to the following equations written for <sup>4</sup>He and <sup>3</sup>He, respectively:

$$(1 - \alpha)mC_{He1}^{in} + \alpha mC_{He2}^{in} + Q_{He} = mC_{He}^{out} + Q_{He}^{dif} \quad (1)$$

$$(1 - \alpha)mR_1^{in}C_{He1}^{in} + \alpha mR_2^{in}C_{He2}^{in} + RQ_{He} = mR^{out}C_{He}^{out} + Q_{3He}^{dif} \quad (2)$$

where  $m$  is the amount of water/ice exchanged per unit of time,  $\alpha$  is the water runoff fraction, and  $R_1^{in}$ ,  $R_2^{in}$  and  $R^{out}$  are the isotope ratios of melted glacier ice, runoff basal water, and accreted ice respectively.  $R$  is the isotope ratio of the helium source  $Q_{He}$ , and  $Q_{He}^{dif}$  and  $Q_{3He}^{dif}$  are the amounts of <sup>4</sup>He and <sup>3</sup>He leaving the lake by direct

diffusion through the glacier ice/lake ice interface.

$Q_{3He}^{dif}$  is negligible because the <sup>3</sup>He concentration gradient between the lake ice and the glacier ice is zero within the experimental uncertainties. Hence, combining equations (1) and (2), we can deduce  $R$  by:

$$R = [R_{out}C_{He}^{out} - (1 - \alpha)R_1^{in}C_{He1}^{in} - \alpha R_2^{in}C_{He2}^{in}] / [C_{He}^{out} + (Q_{He}^{dif}/m) - (1 - \alpha)C_{He1}^{in} - \alpha C_{He2}^{in}] \quad (3)$$

$C_{out}$  and  $R_{out}$  can be taken as the mean values in the accreted ice below the interface ( $C_{He}^{out} = 33.9 \pm 2.6 \text{ nmol kg}^{-1}$  and  $R_{out} = (0.25 \pm 0.04)R_a$ ). The glacier ice layer immediately above the interface, between 3,530 and 3,535 m depth, is assumed to be representative of the input of melted glacier ice occurring in the northern part of the lake ( $C_{He1}^{in} = 10.0 \pm 1.3 \text{ nmol kg}^{-1}$  and  $R_1^{in} = (1.03 \pm 0.08)R_a$ ). Although this layer shows no crustal helium tagging, its near-bottom origin is suggested by the occurrence of small size moraine particles at the base of the section: our preliminary study of the dust in the 3,400–3,538 m layer does indeed reveal the presence of particles, 4–20  $\mu\text{m}$  in diameter, which exceed in size the aeolian dust found at Vostok and are interpreted as crustal dust created by glacier work on the western side of the lake. Crustal helium tagging of the basal layer depends on the intensity of the helium flux and on the residence times of the ice resting on the bedrock. We note that the lack of helium crustal signature in a glacier basal layer was also observed in Greenland. The lowermost 200 m of the GISP2 core<sup>6</sup> shows two sharp spikes of crustal helium, but these spikes do not correspond to layers of silty ice, although there is such a layer at the bottom of the core. The author of ref. 6 concludes that the lack of a simple exponential helium profile at the bottom of the core shows that the crustal helium injection does not involve ice resting directly on the bedrock but may represent disturbed ice layers which have had a significantly longer residence time above the bedrock—long enough to accumulate a large amount of crustal helium from below. The helium isotope values of these crustal anomalies<sup>6</sup> ( $C_{He2}^{in} \approx 20 \text{ nmol kg}^{-1}$  and  $R_2^{in} \approx 0.02R_a$ ) are taken as representative of the runoff water that melts at the ice–bedrock interface.

With the above data set and neglecting  $Q_{He}^{dif}/m$ , equation (3) leads to a maximum isotope ratio  $R$  of helium escaping from the lake bottom of  $R = (0.11 \pm 0.05)R_a$  for values of  $\alpha$  of up to 50%. Based on a basal melt rate of a few millimetres per year for the water runoff<sup>1,13</sup>, a hydrological catchment area equal to several times the lake's surface area, and a melt rate of 100  $\text{mm yr}^{-1}$  in the northern half of the lake<sup>11</sup>, the most probable value for  $\alpha$  falls in the range 5–15%, thus leading to an isotope ratio  $R < 0.06R_a$ . This low <sup>3</sup>He/<sup>4</sup>He

**Table 1 Helium isotope data**

Depth (m)	[ <sup>4</sup> He] (nmol kg <sup>-1</sup> )	R/R <sub>a</sub>
Previous sampling (1989–92)*		
116–165	10.4 ± 1.2	0.985 ± 0.011
120–145	11.9 ± 1.4	1.017 ± 0.031
1,252–1264	13.3 ± 0.5	0.943 ± 0.007
2,441–2501	13.2 ± 0.9	0.954 ± 0.015
Deep core sampling (1997)		
3,530	9.5 ± 0.8	1.111 ± 0.005
3,531	8.7 ± 0.8	1.098 ± 0.005
3,535†	9.8 ± 0.8	0.951 ± 0.005
3,535†	11.9 ± 0.8	0.945 ± 0.005
3,540	29.1 ± 0.8	0.282 ± 0.005
3,551	38.4 ± 0.8	0.262 ± 0.005
3,565	36.0 ± 0.8	0.225 ± 0.005
3,568	35.8 ± 0.8	0.235 ± 0.005
3,576	32.1 ± 0.8	0.253 ± 0.005
3,578	34.5 ± 0.8	0.240 ± 0.005
3,580	35.8 ± 0.8	0.327 ± 0.005
3,599	33.1 ± 0.8	0.191 ± 0.005
3,605	31.8 ± 0.8	0.267 ± 0.005
3,608	32.5 ± 0.8	0.219 ± 0.005

Each sample consisted of one piece of ice, typically 10 g, cut from the core immediately following its retrieval (immediate processing of the sample is essential to avoid helium post-coring diffusion<sup>4</sup>). The samples were stored in one inch diameter copper cylinders evacuated for 2 min with a primary pump to 10<sup>-2</sup>–10<sup>-3</sup> torr and sealed with a metal clamp (the helium blank due to air contamination is negligible, < 4.5 × 10<sup>-14</sup> mol). In spite of the strict sampling protocol, some helium is lost during sample preparation. With a total preparation time of 15 min (including 2 min pumping time), we calculate that this post-coring loss could amount to 10%, but with no significant isotope fractionation). Samples were analysed at LSCE (Saclay) using standard procedures<sup>21</sup>.

\* Unpublished data.  
† Duplicate samples.

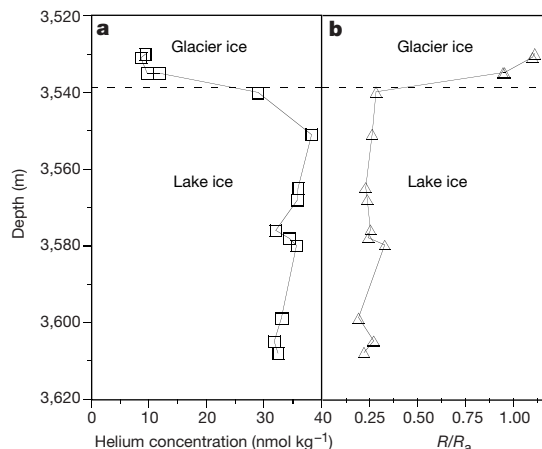


**Figure 1** Measured vertical distribution of helium isotopes across the glacier ice/lake ice boundary (dotted line) at Vostok. **a**, Vertical profile of helium concentration. **b**, Helium isotope ratio  $R = {}^3\text{He}/{}^4\text{He}$ , scaled to the atmospheric ratio  $R_a$ .

ratio is typical of radiogenic crustal helium<sup>6,7</sup>. Taking into account the diffusive term  $Q_{\text{He}}^{\text{dif}}/m$  leads to an even lower estimate.  $^3\text{He}/^4\text{He}$  is a sensitive indicator of mantle involvement in crustal thermal activity<sup>14</sup>. In continental areas of recent tectonic-magmatic activity such as the Yellowstone<sup>15</sup> or Larderello<sup>16</sup> geothermal areas,  $^3\text{He}/^4\text{He}$  is at its highest, accompanied by excess heat flow. On the contrary, in stable areas, where low  $^3\text{He}/^4\text{He}$  ratios are found, the mantle contribution to the heat flow is also low and reaches a minimum value that can be considered as the continental background<sup>8</sup>. Therefore, our data virtually rule out any mantle-derived high-enthalpy hydrothermal manifestations at the bottom of the lake.

Rewriting equation (1) using  $m = M/\tau$ , where  $\tau$  is the renewal time of the lake and  $M$  its mass (with  $M = \rho HS$  where  $\rho$  is the lake mean density,  $H$  the mean depth and  $S$  the average surface area), we obtain:

$$\Phi_{\text{He}} = (C_{\text{He}}^{\text{out}} - (1 - \alpha)C_{\text{He1}}^{\text{in}} - \alpha C_{\text{He2}}^{\text{in}})\rho H/\tau + \Phi_{\text{He}}^{\text{dif}} \quad (4)$$

where  $\Phi_{\text{He}}$  and  $\Phi_{\text{He}}^{\text{dif}}$  are the helium flux from the bedrock and the helium diffusive flux respectively, scaled to the average lake surface area  $S$  ( $\Phi_{\text{He}} = Q_{\text{He}}/S$  and  $\Phi_{\text{He}}^{\text{dif}} = Q_{\text{He}}^{\text{dif}}/S$ ). The diffusive component  $\Phi_{\text{He}}^{\text{dif}}$  can be estimated from the helium concentration gradient across the glacier ice/lake ice interface ( $\nabla C$ ) and the helium diffusion coefficient ( $D_{\text{He}}$ ) by  $\Phi_{\text{He}}^{\text{dif}} = D_{\text{He}} \times \nabla C$ . Taking for  $\nabla C$  the concentration gradient measured at Vostok across the glacier ice/lake ice boundary ( $\nabla C \approx 3.8 \mu\text{mol m}^{-4}$ ), and a diffusion coefficient  $D_{\text{He}} = 5 \times 10^{-6} \text{ cm}^2 \text{ s}^{-1}$  (refs 3, 17, 18) at the temperature of the interface ( $T = -3^\circ\text{C}$ ), we calculate a diffusive flux of  $60 \text{ nmol m}^{-2} \text{ yr}^{-1}$ . If we adopt for  $\Phi_{\text{He}}$  the average estimate for the continental crust of  $1.46 \mu\text{mol m}^{-2} \text{ yr}^{-1}$  assuming that the helium loss from crust is equal to production<sup>14</sup>, it follows that the first term of equation (4) (advective component) equals  $1.4 \mu\text{mol m}^{-2} \text{ yr}^{-1}$ , leading to a residence time  $\tau$  ranging from 4,800 to 5,000 years (taking  $\alpha$  between 5% and 15% and a mean lake depth of 300 m; ref. 19).

This residence time corresponds to a lake mean melting/accretion rate  $h = 2(1 - \alpha)H/\tau$  of  $11 \text{ cm yr}^{-1}$  (if the respective surface area of melting and freezing are assumed to be roughly equal). This value is of the same order of magnitude as that inferred from airborne 60-MHz radar transects above the lake<sup>11</sup>. Owing to the low heat flux measured at Vostok, corresponding to a maximum apparent accretion rate of  $4 \text{ mm yr}^{-1}$  (ref. 20), this high accretion rate implies that upon freezing, most of the latent heat is released within the lake water itself rather than in the overlying ice. This is consistent with the recent hypothesis of Souchez *et al.*<sup>12</sup>, who suggest that the main mechanism responsible for lake ice formation is loose frazil ice crystals produced in supercooled waters rising along the tilted ice-water interface.

In reasonable agreement with geophysical inferences<sup>11</sup> indicating the significant water exchange between the base of the ice sheet and the lake waters, helium data in the deep Vostok ice core point to appreciable mass exchange occurring between the subglacial lake and the overlying ice sheet. More importantly, the helium isotope data virtually eliminates any significant high-enthalpy hydrothermal input to the energy budget available for metabolic activity within the lake, an important issue with regards to the sustainability of life in this isolated environment. □

Received 1 December 2000; accepted 13 March 2001.

- Kapitsa, A. P., Ridley, J. K., Robin, G. Q., Siegert, M. J. & Zotikov, I. A. A large deep freshwater lake beneath the ice of central East Antarctica. *Nature* **381**, 684–686 (1996).
- Jouzel, J. *et al.* More than 200 meters of lake ice above subglacial lake Vostok, Antarctica. *Science* **286**, 2138–2141 (1999).
- Haas, J., Bullemer, B. & Kahane, A. Diffusion de l'hélium dans la glace monocristalline. *Solid State Commun.* **9**, 2033–2035 (1971).
- Jean-Baptiste, P., Raynaud, D., Mantsi, F., Sowers, T. & Barkov, N. Measurement of helium isotopes in Antarctic ice: preliminary results from Vostok. *CR Acad. Sci. Paris* **316**, 491–497 (1993).
- Craig, H. & Chou, C. C. Helium isotopes and gases in Dye 3 ice cores. *Eos* **63**, 298 (1982).
- Craig, H. in *Abstr. Int. Conf. On Stable Isotopes and Isotope Effects* (eds Soulié, E. & Roth, E.) 1–112 (Commissariat à l'Énergie Atomique, Paris, 1999).
- Andrews, J. N. The isotopic composition of radiogenic helium and its use to study groundwater movement in confined aquifers. *Chem. Geol.* **49**, 339–351 (1985).

- Mamyrin, B. A. & Tolstikhin, I. N. *Helium Isotopes in Nature* (Elsevier, Amsterdam, 1984).
- Craig, H. & Lupton, J. E. Primordial neon, helium and hydrogen in oceanic basalts. *Earth Planet. Sci. Lett.* **31**, 369–385 (1976).
- Farley, K. A. & Neroda, E. Noble gases in the Earth's mantle. *Annu. Rev. Earth Planet. Sci.* **26**, 189–218 (1998).
- Siegert, M. J., Kwok, R., Mayer, C. & Hubbard, B. Water exchange between the subglacial Lake Vostok and the overlying ice sheet. *Nature* **403**, 643–646 (2000).
- Souchez, R., Petit, J. R., Tison, J. L., Jouzel, J. & Verbeke, V. Ice formation in subglacial Lake Vostok, Central Antarctica. *Earth Planet. Sci. Lett.* **181**, 529–538 (2000).
- Savvin, A., Greve, R., Calov, R., Mugge, B. & Hutter, K. Simulation of the Antarctic ice sheet with a three-dimensional polythermal ice-sheet model, in support of the EPICA project. II. Nested high resolution treatment of Dronning Maud Land, Antarctica. *Ann. Glaciol.* **30**, 69–75 (2000).
- O'Nions, R. K. & Oxburgh, E. R. Heat and helium in the earth. *Nature* **306**, 429–431 (1983).
- Craig, H., Lupton, J. E., Welhan, J. A. & Poreda, R. Helium isotope ratios in Yellowstone and Lassen Park volcanic gases. *Geophys. Res. Lett.* **5**, 897–900 (1978).
- Hooker, P. J., Bertrami, R., Lombardi, S., O'Nions, R. K. & Oxburgh, E. R. Helium-3 anomalies and crust-mantle interaction in Italy. *Geochim. Cosmochim. Acta* **49**, 2505–2513 (1985).
- Davy, J. G. & Miller, K. W. The diffusion of helium through ice. *Solid State Commun.* **3**, 1459–1461 (1970).
- Jones, S. J. Diffusion of helium in ice. *Phys. Canada* **27**, 60–61 (1971).
- Siegert, M. J. Antarctic subglacial lakes. *Earth Sci. Rev.* **50**, 29–50 (2000).
- Salamatin, A., Vostretsov, R. N., Petit, J. R., Lipenkov, V. Y. & Barkov, N. I. Geophysical and paleoclimatic implications of the temperature profile from the deep borehole at Vostok station (Antarctica). *Data Glaciol. Stud.* **85**, 233–240 (1998).
- Jean-Baptiste, P., Mantsi, F., Dapoigny, A. & Stievenard, M. Design and performance of a mass spectrometric facility for measuring helium isotopes in natural waters and for low-level tritium determination by the  $^3\text{He}$  ingrowth method. *Appl. Radiat. Isot.* **43**, 881–891 (1992).

Acknowledgements

Vostok is a joint project between Russia, France and the USA. We thank the Russian Antarctic Expedition for station and drilling-operation support, and the IFRTP (Institut Français de Recherche et Technologies Polaires) and the NSF Office of Polar Program for logistic support. The project was supported in Russia by the Russian Ministry of Sciences, and in France by CNRS and CEA. We thank A. Salamatin, P. Duval and J. Meyssonier for discussions.

Correspondence should be addressed to P.J.-B. (e-mail: pjb@lsce.saclay.cea.fr).

Earthquake triggering by seismic waves following the Landers and Hector Mine earthquakes

J. Gomberg\*, P. A. Reasenbergt, P. Bodin‡ & R. A. Harris†

\* US Geological Survey, Center for Earthquake Research and Information, 3876 Central Avenue Suite 2, Memphis, Tennessee 38152-3050, USA

† US Geological Survey, MS 977, 345 Middlefield Road, Menlo Park, California 94025, USA

‡ Center for Earthquake Research and Information, The University of Memphis, 3876 Central Avenue, Suite 1, Memphis, Tennessee 38152-3050, USA

The proximity and similarity of the 1992, magnitude 7.3 Landers and 1999, magnitude 7.1 Hector Mine earthquakes in California permit testing of earthquake triggering hypotheses not previously possible. The Hector Mine earthquake confirmed inferences that transient, oscillatory 'dynamic' deformations radiated as seismic waves can trigger seismicity rate increases, as proposed for the Landers earthquake<sup>1–6</sup>. Here we quantify the spatial and temporal patterns of the seismicity rate changes<sup>7</sup>. The seismicity rate increase was to the north for the Landers earthquake and primarily to the south for the Hector Mine earthquake. We suggest that rupture directivity results in elevated dynamic deformations north and south of the Landers and Hector Mine faults, respectively, as evident in the asymmetry of the recorded seismic velocity fields. Both dynamic and static stress changes seem important for triggering in the near field with dynamic stress changes dominating at greater distances. Peak seismic velocities recorded for each earthquake suggest the existence of, and place bounds on,